Measurement of radiative proton capture on ^{18}F and implications for oxygen-neon novae reexamined

C. Akers, A. M. Laird, B. R. Fulton, C. Ruiz, D. W. Bardayan, L. Buchmann, G. Christian, B. Davids, L. Erikson, J. Fallis, U. Hager, D. Hutcheon, L. Martin, A. St. J. Murphy, K. Nelson, D. Ottewell, A. Rojas, and A. Spyrou

Measurement of Radiative Proton Capture on ^{18}F and Implications for Oxygen-Neon Novae

C. Akers,[1, 2, *] A.M. Laird,[2] B.R. Fulton,[2] C. Ruiz,[1] D.W. Bardayan,[3, †] L. Buchmann,[1]
G. Christian,[1, ‡] B. Davids,[1] L. Erikson,[4] J. Fallis,[1] U. Hager,[5, §] D. Hutcheon,[1]
L. Martin,[1] A. St.J. Murphy,[6] K. Nelson,[7] D. Ottewell,[1] A. Rojas,[1] and A. Spyrou[8, 9, 10]

[1] *TRIUMF, Vancouver, British Columbia V6T 2A3, Canada*
[2] *Department of Physics, University of York, York YO10 5DD, United Kingdom*
[3] *Physics Division, Oak Ridge National Laboratory, Oak Ridge, Tennessee 37831, USA*
[4] *Pacific Northwest National Laboratory, Washington 99354, USA*
[5] *Colorado School of Mines, Colorado 80401, USA*
[6] *SUPA, School of Physics and Astronomy, The University of Edinburgh, Edinburgh EH9 3JZ, United Kingdom*
[7] *McMaster University, Hamilton, Ontario L8S 4L8, Canada*
[8] *National Superconducting Cyclotron Laboratory, Michigan State University, East Lansing, Michigan 48824, USA*
[9] *Department of Physics & Astronomy, Michigan State University, East Lansing, Michigan 48824, USA*
[10] *Joint Institute of Nuclear Astrophysics, Michigan State University, East Lansing, Michigan 48824, USA*

Background: The rate of the ^{18}F$(p,\gamma)^{19}$Ne reaction affects the final abundance of the radioisotope ^{18}F ejected from novae. This nucleus is important as its abundance is thought to significantly influence the first stage 511 keV and continuum γ-ray emission in the aftermath of novae. No successful measurement of this reaction existed prior to this work, and the rate used in stellar models had been calculated based on incomplete information from contributing resonances.

Purpose: Of the two resonances thought to provide a significant contribution to the astrophysical reaction rate, located at $E_{\mathrm{c.m.}}$=330 and 665 keV, the former has a radiative width estimated from the assumed analogue state in the mirror nucleus, ^{19}F, while the latter resonance does not have an analogue state assignment at all, resulting in an arbitrary radiative width being assumed. As such, a direct measurement was needed to establish what role this resonance played in the destruction of ^{18}F at nova temperatures. This paper extends and takes the place of a previous Letter which reported the strength of the $E_{\mathrm{c.m.}}$=665 keV resonance.

Method: The DRAGON recoil separator was used to directly measure the strength of the important 665 keV resonance in this reaction, in inverse kinematics, by observing ^{19}Ne reaction products. Radioactive ^{18}F beam was provided by the ISAC facility at TRIUMF. R-matrix calculations were subsequently used to evaluate the significance of the results at astrophysical energies.

Results: We report the direct measurement of the ^{18}F$(p,\gamma)^{19}$Ne reaction with the re-evaluation of several detector efficiencies and the use of an updated ^{19}Ne level scheme in the reaction rate analysis. The strength of the 665 keV resonance (E_x=7.076 MeV) is found to be an order of magnitude weaker than currently assumed in nova models. An improved analysis of the previously reported data is presented here, resulting in a slightly different value for the resonance strength. These small changes, however, do not alter the primary conclusions.

Conclusions: Reaction rate calculations definitively show that the 665 keV resonance plays no significant role in the destruction of ^{18}F at novae temperatures.

I. INTRODUCTION

Novae are among the most frequent and energetic explosive astrophysical events in our Universe [1]. They are thought to occur as the result of H-rich mass accretion onto the surface of a white dwarf from a companion red giant or main sequence star in a binary system.

A thermonuclear runaway is initiated in the subsequent high pressure and temperature electron degenerate environment, causing an outburst of the previously accreted material [1]. Many questions surrounding these events remain unanswered, and additional observational constraints are needed for greater clarification.

Such constraints may be possible with the advent of satellite based γ- and X-ray spectroscopy; we can now observe the decay of radioisotopes from astrophysical sites, such as novae, providing a powerful tool to probe the processes occurring during the lives and deaths of stars. These missions can provide valuable experimental data on the abundances of radioisotopes synthesized in astrophysical environments and thus put stringent constraints on astrophysical models. A recent example is the INTEGRAL observation of hard X-rays from Supernova 1987A [2], which allowed for the amount of ^{44}Ti produced during the core collapse explosion to be estimated. Such observations are crucial tests of nucleosynthesis models.

---

* Present address: Rare Isotope Science Project, Institute for Basic Science, 70, Yuseong-daero 1689-gil, Yusung-gu, Daejeon 305-811, Korea; cakers@ibs.re.kr
† Present address: Department of Physics, University of Notre Dame, Notre Dame, Indiana 46556, USA
‡ Present address: Cyclotron Institute & Department of Physics and Astronomy, Texas A&M University, College Station, Texas 77843, USA
§ Present address: National Superconducting Cyclotron Laboratory, Michigan State University, East Lansing, Michigan 48824, USA

A. Classical novae

While there has been no definitive observation of nuclear-decay produced γ-rays from nova outbursts, such γ-ray spectroscopy is anticipated in the future. Hence there is significant interest in radioisotopes thought to be abundantly produced in such events, in the hope that their decay signatures can be directly observed. One radioisotope of interest is ^{18}F, as its positron annihilation, following β^+ decay, is thought to be the major source of 511 keV line emission γ-rays after nova outbursts [3]. This is due to the fact that the relatively long half life of ^{18}F ($t_{1/2}$=110 mins) results in a significant number of positrons being emitted shortly after the expanding nova envelope becomes transparent to γ-rays, whilst its half-life is short enough that its absolute decay rate remains high. If the ^{18}F production and destruction rates are sufficiently well known then observations of this nuclide's γ-ray emission can provide constraints on physical conditions inside novae, leading to improvements in astrophysical models. Such models require additional experimental data to help address discrepancies in their predictions with observations. Observation of the 511 keV γ-ray line emission is complicated by the need for difficult *a posteriori* searches of γ-ray telescope data motivated by wide field γ-ray or X-ray telescope identifications of novae, due to the peak optical brightness occurring days after the positron annihilation flash [4, 5]. Two types of white dwarf stars, carbon-oxygen (CO) and oxygen-neon (ONe), are thought to be responsible for novae and are therefore of great interest for any future satellite observations. CO nova models predict a peak temperature of $\approx$0.15 GK, whilst ONe nova models predict a hotter peak temperature range of between $\approx$0.23 and $\approx$0.42 GK [6].

B. Previous studies

Understanding both the production and destruction rates of ^{18}F at nova temperatures is critical for the aforementioned reasons. One of the main uncertainties in this radioisotope's final abundance depends on its destruction rate via the (p,γ) and (p,α) channels. The ^{18}F$(p,\alpha)^{15}$O reaction is estimated to be a few thousand times faster [7] and therefore it has been the focus of many previous studies [8–10] (and references therein). Little effort has gone into the study of the ^{18}F$(p,\gamma)^{19}$Ne reaction however, based on its much lower estimated cross section and the limited availability of sufficiently intense radioactive beams. A sensitivity study by Iliadis *et al.* [6] indicates that, for ONe novae, a factor of 10 increase or decrease in the (p,γ) rate changes the calculated abundance of ^{18}F by a factor of 2.5 or 0.9, respectively. This significantly affects the potential number of novae whose 511 keV γ-ray line emission is detectable via satellite missions. Therefore, given the recent improvements in knowledge of the (p,α) rate, it is important that effort is made in tandem to reduce the uncertainty in the (p,γ) reaction rate.

The ^{18}F$(p,\gamma)^{19}$Ne reaction proceeds through an excitation range in ^{19}Ne containing states whose precise parameters are not currently fully determined. Although not all states expected to occur in the relevant energy region ($\approx E_{c.m.}$=-0.2→0.7 MeV; this energy interval is greater than what would be expected from a simple Gamow window calculation due to the interference effects of broad states in ^{19}Ne, see section III I) have been observed, it was previously thought that the $E_{c.m.}$=330 keV (E_x=6.741 MeV) resonance was the main contributor to the reaction rate in novae, together with the 665 keV (7.076 MeV) resonance at the higher temperatures reached in ONe models [7, 11, 12]. There is also a non-resonant contribution that becomes influential at lower novae temperatures and is considered in Refs [7, 12, 13].

The α-particle and proton partial widths (Γ_α and Γ_p) are well known for the 665 keV resonance [14], however, the radiative width Γ_γ has only a single experimental upper limit, set by Rehm *et al.* [13]. The lack of an analogue state assignment [15] means no reliable estimate can be made. The experimental upper limit does not significantly constrain the reaction rate contribution of this state at nova temperatures and an arbitrary value of 1 eV [14] was therefore assumed in the literature, taken from surrounding states in ^{19}F.

Similarly, Γ_γ of the 330 keV resonance has not been determined experimentally and a value of 5.0±2.6 eV is used based on an assumed analogue assignment [14]. This assignment was determined via comparison of the populated states in ^{19}F and ^{19}Ne, in a mirror reaction study by Utku *et al.* [7]. The quoted Γ_α (effectively the total width in this case) of 5.2±3.7 keV is also based on this same analogue assignment. By contrast, a direct measurement of the ^{18}F$(p,\alpha)^{15}$O cross section [16] allowed the Γ_p to be experimentally determined (Γ_p=2.22±0.69 eV). A Γ_p of 7.3±0.6 eV was extracted from proton transfer data [10], however, the population of the 330 keV resonance could have been contaminated by nearby states.

Recent ^{19}F(^{3}He,t)^{19}Ne and ^{20}Ne$(p,d)^{19}$Ne studies by Laird *et al.* [17] and Bardayan *et al.* [18], respectively, found discrepancies in the spin and parity assignments for levels close to the proton threshold in ^{19}Ne. This may have ramifications for the ^{18}F$(p,\gamma)^{19}$Ne reaction rate at nova temperatures; the new spin and parity assignments differ from those published previously, leading to changes in the interference effects with stronger, higher lying states, hence altering the capture cross section. In summary, key parameters of both these resonances are experimentally unconstrained and therefore the ^{18}F$(p,\gamma)^{19}$Ne reaction rate, and its impact on ^{18}F abundance, must be regarded as very uncertain.

The present authors reported a direct observation of the strength of the resonance located at $E_{c.m.}$=665 keV in a recent Letter [19]. However, this paper extends and supersedes that work due to the re-evaluation of several detector efficiencies and the use of an updated ^{19}Ne level scheme in the reaction rate analysis.

II. EXPERIMENTAL FACILITIES AND PROCEDURE

The experiment was carried out at the DRAGON (Detector of Recoils and Gammas Of Nuclear reactions) facility, located in the ISAC I hall at TRIUMF. DRAGON is a specialized facility designed to study radiative proton and α capture reactions at sub-Coulomb barrier energies in inverse kinematics, as illustrated in Fig. 1. It consists of three main sections, 1) a differentially pumped windowless gas target chamber surrounded by a high efficiency BGO γ array; 2) a high suppression two-stage electromagnetic separator; and 3) a heavy ion detector system. The heavy ion detection system, located downstream of the final focus of the separator, consists of two micro-channel plate detectors (MCP), used for measuring recoil time of flight, and a multi-anode ionization chamber (IC), used for measuring recoil energy loss. For a more detailed discussion of the DRAGON facility the reader is referred to Refs [20, 21].
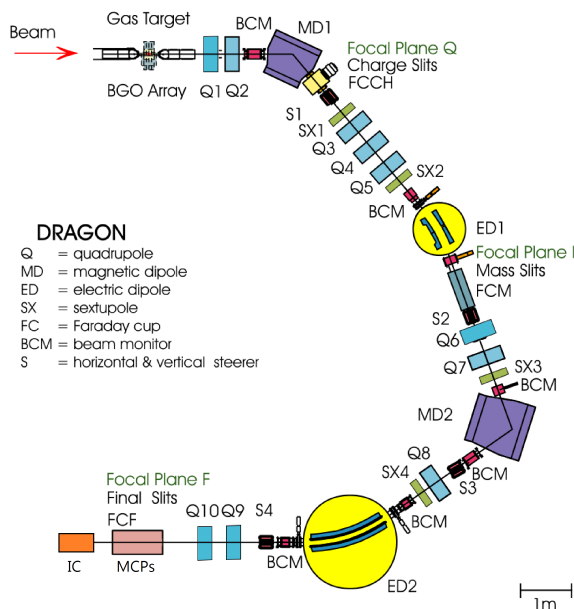

FIG. 1. Scale drawing outline of DRAGON's recoil separator showing the location of important elements relative to the gas target. Adapted and reprinted with permission from [21]. Copyright 2007 by the American Physical Society.

A. Gas target system

The beam entered DRAGON via a windowless gas target that was filled with hydrogen and is capable of maintaining pressures up to 10 Torr. The distance between the two innermost apertures is 11.05±0.01 cm, although the gas volume's effective length was measured to be 12.3±0.4 cm [20]. The long target ensured that

the resonance of interest resided within the target region due to the large beam energy loss across its length. Two silicon detectors were located inside the target chamber for the purpose of monitoring beam intensity via elastic scattering on the target nuclei. The target gas pressure is monitored via a manometer connected to the target gas cell. There was also an array of high efficiency BGO detectors surrounding the chamber, used for detecting γ-rays coincident with heavy ion events. A drawing of DRAGON's target chamber is shown in Fig. 2.
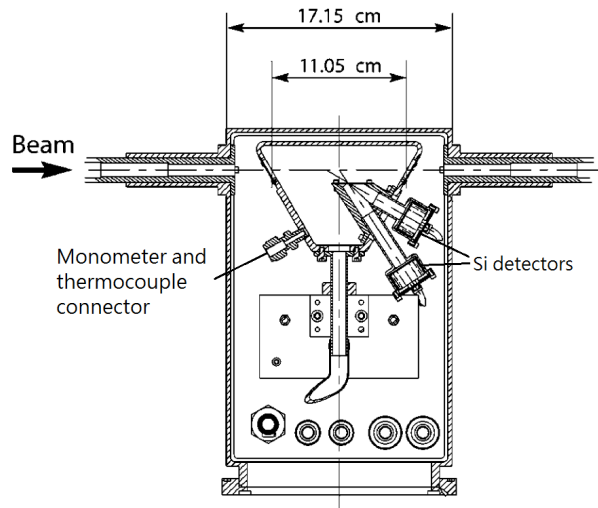

FIG. 2. Schematic drawing of the target chamber box at DRAGON. The central gas cell, located inside of the rectangular outer chamber box, is distinguished by its trapezoidal shape. Gas is fed into the target from the bottom of the gas cell. Two silicon detectors, located just downstream of the center of the target and angled at 30 and 57 degrees to the beam line, are used to monitor the rate of beam induced elastic scattering on the target. Target pressure and temperature are monitored via a monameter and thermocouple connected to the central cell. Adapted and reprinted with permission from [24]. Copyright 2004 by the American Physical Society.

B. Particle identification detectors

DRAGON was equipped with two secondary electron emission monitors instrumented with micro channel plate detectors that allowed for time of flight measurements of incident ions. The use of MCPs, capable of separating ions of different masses through their time of flight difference, enhanced overall particle identification. Diamond like carbon foils (DLC) were placed in the beam line, directly below the MCPs, for electron generation. They were sufficiently thin (20 μg/cm^2) so as to not interfere appreciably with the recoil ion energy or trajectory. This allowed the MCP system to be used in parallel with the ionization chamber, located directly downstream (see
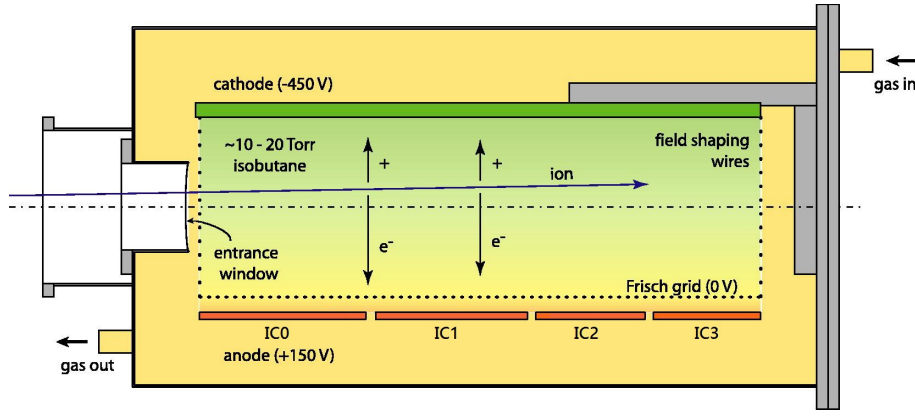
FIG. 3. Schematic drawing of the ionization chamber used for recoil particle identification at the end of the DRAGON separator. Four anodes were located sequentially along the recoil path, allowing for ΔE measurements. Reprinted from Ref. [23], Copyright 2008, with permission from Elsevier.
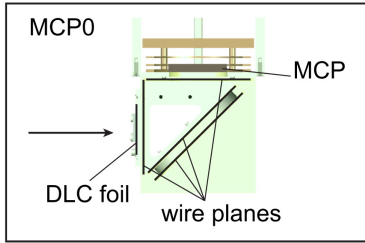

FIG. 4. Schematic drawing of the first MCP detection system, the second was located 59 cm downstream allowing for local TOF measurments. Biased wire planes were used to deflect electrons generated from the DLC foil onto the MCP detectors. Reprinted from Ref. [22], Copyright 2009, with permission from Elsevier.

Ref. [22] for more details on this detection system). Biased wire planes were also used to deflect the electrons upwards, towards the MCPs, see Fig. 4.

The ionization chamber (IC) at DRAGON consisted of an isobutane gas volume containing four separate anode plates for charge collection, with a thin (1 to 2 μm thick) Mylar foil covering the chamber's entrance. The four anodes (referred to as IC0, IC1, IC2 and IC3, ordered sequentially in position from front to back) along its length allowed for ion energy loss to be characterized as a function of depth, see Fig. 3.

C. Beam production and delivery

The ^{18}F beam was sourced using a 500 MeV proton beam, from the TRIUMF cyclotron, incident on a silicon carbide target. Spallation reactions on the target nuclei produced a variety of nuclear species, including ^{18}F. A=18 products were extracted, ionized in a FEBIAD ion source [25] and subsequently filtered us-

ing a high resolution mass separator [26]. The beam was then sent to the ISAC-I experimental hall radio frequency quadrupole linear accelerator then through a carbon stripper foil and into the ISAC drift tube linear accelerator. From here the radioactive beam was directed into the DRAGON gas target. An average ^{18}F^{4+} beam intensity of 1.74×10^6 ions/sec was delivered to the experiment, as determined by the two silicon scattering detectors located inside the target chamber (see section III D). A laboratory beam energy per nucleon of 0.717 MeV/u was chosen, to place the $E_{\text{c.m.}}$=665 keV resonance near the center of the target. Initially the separator was tuned to transmit attenuated beam, for the purposes of determining the optimal tune for recoil products formed inside the target. The attenuated beam was identical to un-attenuated beam but lower in intensity so as not to damage any of DRAGON's detectors or diagnostic devices.

The purity of the ^{18}F beam was characterized with the IC at the end of DRAGON. It was possible to distinguish between the ^{18}F ions and accompanying ^{18}O ion contaminants via the IC energy spectrum, as the ^{18}O ions had a smaller rate of energy loss in isobutane gas. Additional stable beam ^{18}O runs allowed for DRAGON's optical tuning to be assessed in the presence of high intensity beam similar in mass and charge to that of ^{18}F. The ^{18}O beam also allowed for the characterization of ^{19}F recoil events (see section III E).

The recoil separator was subsequently tuned to accept recoiling ^{19}Ne ions in their most abundant charge state, initially estimated to be 6$^+$ via the parameterization of Ref. [27], as was later confirmed experimentally (see section III A). The maximum recoil cone angle was calculated to be 11 mrad, well within DRAGON's acceptance [20]. In total, the effective beam time on target was 6.6 days.

III. ANALYSIS AND RESULTS

Extracting experimental parameters, such as the resonance strength ($\omega\gamma$) and the radiative partial width (Γ_γ), required determining the experimental yield fraction, Y, given by

$$Y = \frac{N_{\mathrm{r}}^{\mathrm{tot}}}{N_{\mathrm{b}}} \qquad (1)$$

where N_{b} is the total number of beam ions incident on target and $N_{\mathrm{r}}^{\mathrm{tot}}$ is the total number of recoils produced, for the whole duration of the run. In order to calculate the latter, the number of observed recoils ($N_{\mathrm{r}}^{\mathrm{det}}$) had to be corrected for a number of factors, including: efficiency of transmission through the separator (ϵ_{ERS}); recoil charge state fraction (ϵ_{CSD}); MCP detection efficiency (ϵ_{MCP}); efficiency of the end detector (ϵ_{det}) and data acquisition live time efficiency (ϵ_{LT})

$$N_{\mathrm{r}}^{\mathrm{tot}} = \frac{N_{\mathrm{r}}^{\mathrm{det}}}{\epsilon_{\mathrm{ERS}}\,\epsilon_{\mathrm{CSD}}\,\epsilon_{\mathrm{MCP}}\,\epsilon_{\mathrm{det}}\,\epsilon_{\mathrm{LT}}} \qquad (2)$$

From the yield, the resonance strength of the excitation level of interest could then be extracted, via the equation [28]

$$\omega\gamma = \frac{2\pi}{\lambda^2(E_{\mathrm{r}})} \frac{\epsilon(E_{\mathrm{r}})}{Y} \times$$
$$\left[\arctan\left(\frac{E_0 - E_{\mathrm{r}}}{\Gamma/2}\right) - \arctan\left(\frac{E_0 - E_{\mathrm{r}} - \Delta E}{\Gamma/2}\right) \right]^{-1} \qquad (3)$$

where λ is the reaction system's de Broglie wavelength, ϵ is the stopping power, E_{r} is the resonance energy, E_0 is the initial center of mass energy and ΔE is the beam energy loss across the length of the target. All quantities are evaluated in the center of mass frame of reference. The target stopping power was deduced from

$$\epsilon(E) = -\left(\frac{\mathrm{N_t}}{\mathrm{V}}\right)^{-1} \frac{\mathrm{d}E}{\mathrm{d}x} \qquad (4)$$

where $\frac{\mathrm{N_t}}{\mathrm{V}}$ is the target number density (the number of target nuclei per unit volume) and $\frac{\mathrm{d}E}{\mathrm{d}x}$ is the rate of beam energy loss through the target in the center of mass coordinate system. The former quantity was determined from the central target gas pressure, which was constantly monitored and maintained within the range 7.3 to 7.6 Torr. This value was chosen to ensure as much of the resonance was contained within the target region as possible. Energy loss was determined using the first dipole magnet of the separator to measure the beam energy, with and without gas in the target. However, this

method was not possible with the ^{18}F beam, see section III D.

Partial widths, used for calculating cross sections and reaction rates, were deduced using the relationship [28]

$$\omega\gamma = \frac{(2J_{\mathrm{R}} + 1)}{(2J_{\mathrm{p}} + 1)(2J_{18\mathrm{F}} + 1)} \frac{\Gamma_{\mathrm{p}}\Gamma_\gamma}{\Gamma} \qquad (5)$$

where J_{R}, J_{p} and $J_{18\mathrm{F}}$ are the spins of the resonance of interest, target proton nuclei and the ^{18}F ground state, respectively (in units of $\hbar$).

A. Charge state distributions

As only one recoil charge state could be transmitted through DRAGON for a given run, it was necessary to determine what fraction of all recoil ions produced were in the selected charge immediately before they entered MD1 (ϵ_{CSD}). Charge state distributions were measured by tuning ^{20}Ne beam in the charge state of interest through the gas target and MD1. Faraday cup readings both up- and down-stream of MD1 then provided a measure of each charge state's relative intensity. The beam emittance, typically <5 mrad, was much smaller than the separator's acceptance (20 mrad) and MD1 was operated far from saturation, ensuring 100% transmission of the selected charge state. As an ion beam's charge state distribution in a medium is dominated by its atomic number and speed, ^{20}Ne provided an acceptable surrogate for the charge state abundance of the ^{19}Ne ions produced in the reaction. Measurements of ^{20}Ne charge state distributions were taken at multiple pressures (1, 4.5 and 7.5 Torr) so as to account for any possible effects from the residual gas outside of the main target chamber. The standard deviation in the measurements is then adopted as the systematic uncertainty in the given charge state fraction. The ^{20}Ne beam energy corresponded to the ion speed of recoil products from the earlier ^{18}F run, and the mean 6^+ charge state fraction was found to be ϵ_{CSD}=23.3±1.1%.

B. Detector efficiencies

The detection efficiency of the MCPs was calculated using attenuated beam data, by dividing the number of events that had both a good MCP time of flight and IC energy loss value ($N_{\mathrm{MCP\&IC}}$) by the total number of good IC events (N_{IC}):

$$\epsilon_{\mathrm{MCP}} = N_{\mathrm{MCP\&IC}}/N_{\mathrm{IC}} \qquad (6)$$

Such a calculation depends on using N_{IC} as an absolute measure of the number of ions incident on the MCP detectors. It would be expected that the same logic be used when calculating the IC efficiency, such that

$\epsilon_{IC} = N_{MCP\&IC}/N_{MCP}$. However, the situation was complicated by the presence of a mesh supporting the DLC foils, together with the biased wire planes, used in the MCP detectors located upstream. As these partially obscured the beam line, there was the possibility that an ion may hit the mesh on the second MCP and generate enough electrons to produce an MCP signal without traversing the detector. As such, there was no accurate measure of how many ions were incident on the IC window. To account for this, the ratio $N_{MCP\&IC}/N_{MCP}$ was multiplied by the geometric transparency of both MCP detector meshes (65.5%) to determine the lowest possible end detector efficiency (defined here as the combined IC efficiency and MCP mesh transmission, (ϵ_{det}). The corresponding highest end detector efficiency could be calculated by multiplying the same ratio by the geometric transparency of only the first MCP mesh (80.9%). ϵ_{det} was then taken as the mean of the two extreme possible efficiencies (64.6% and 52.2%) and its uncertainty taken as 68% of the range so as to give a 1σ coverage, yielding ϵ_{det}=58.4±4.2%.

C. Beam energy loss

Energy loss data were required to accurately characterize the beam energy profile across the depth of the target (see section III D). The standard procedure for such measurements involved tuning the beam through MD1 with the aid of current monitors located in the beam line. However, due to the low beam intensity this method was not feasible, and so SRIM-2013.00 [29] was used to calculate energy losses for the ^{18}F beam. The program yielded an energy loss 4.3% higher than that measured experimentally for the ^{18}O beam run, constituting good agreement considering there was an uncertainty of 3.3% in the target's overall length [20]. Inspection of SRIM's experimental database for all ion stopping powers in hydrogen targets yielded a mean discrepancy between experimental data and theoretical calculations of 8.1%. This value was then adopted as an estimate for the uncertainty in SRIM's calculated energy loss. The effects of variations in pressure during the run, which affected the beam energy loss, were minimal; the measurements had a standard deviation of magnitude 1.3% of the mean value (7.45±0.10 Torr). Combined in quadrature with the SRIM uncertainty, a total uncertainty of 8.4% for the energy loss of ^{18}F ions through DRAGON's target was adopted. A final laboratory energy loss of 474±40 keV resulted, corresponding to 25.0±2.1 keV in the center of mass frame.

D. Beam normalization

In DRAGON measurements, the total number of incident beam particles (N_b) is usually determined by normalizing the measured rate of target nuclei elastically scattered by the beam, into either of the two silicon detectors mounted inside the target assembly, to Faraday Cup (FC) readings from just before and after the target [24]. The detector at 30° to the beam line was typically used since the other detector, angled at 57°, suffered from significant low energy noise that obscured the scattering peak. However, due to the low beam intensity, the FCs could not provide a reliable current measurement and so an alternative approach was employed, using a Monte Carlo simulation of the gas target. The reasoning behind constructing such a simulation was that the total number of incident beam ions on target should be directly proportional to the number of elastically scattered target protons observed by the silicon detectors (N_p), for a given experiment (assuming consistency in target composition, which is the case with DRAGON). Hence the ratio N_b/N_p should remain constant. By simulating the specific kinematic, geometric and physical conditions of beam induced elastic scattering in the target chamber it was postulated that this ratio could be calculated.

This approach required the cross section for elastic scattering and beam energy profile across the depth of the target. However, due to the presences of several resonances in the energy region of interest, the elastic scattering cross section could not be modeled as purely Rutherford in nature. Calculations from an R-matrix fit to the experimental data given in Ref. [8] were used instead. Inspection of the experimental data points and their associated uncertainty revealed a cross section measurement uncertainty on the order of 6.5% in the relevant energy region. This value was hence used as an estimate of the systematic uncertainty of the input cross section data.

With the aid of the cross section and energy loss data, the Monte Carlo simulation then enabled the ratio N_b/N_p to be determined. Variations in beam position and angle were considered, ±2 mm and ±2 mrad, based on typical ISAC beam quality and the extremities that would allow for the beam to be transmitted through the target cell. Variations in beam energy, based on the accuracy of the energy loss data were also considered (see III C). The ratio N_b/N_p was most sensitive to the beam position; variations in beam energy loss and angle had minimal effect. These beam parameter variations were compared to the case of a centered beam, resulting in a maximum deviation of 10% in the calculated N_b/N_p ratio. This was then adopted for the simulation's accuracy. Adding this in quadrature with the cross section uncertainty gave a total uncertainty of 12% in the beam normalization analysis. The level of ^{18}O beam contamination was so small, less than 1 part in 20, that it was ignored in the simulation (see section III E). Given that the total uncertainty in the reaction yield was dominated by the low count rate of recoil events such approximations in the beam normalization and its uncertainty were of minimal consequence with regards to the final result however. Analysis of the experimental scattering data then yielded a value for N_p, which was subsequently used to calculate

the total integrated beam intensity on target, yielding a value of $N_b = (9.8 \pm 1.2) \times 10^{11}$ ^{18}F ions.

The experimental silicon detector spectrum compared well with that from the simulation, as the latter was able to replicate the energy distribution's width, illustrated in Fig. 5. The experimental data were calibrated linearly in energy from the simulation results and so the accurate replication of energy spread indicates that the simulation was accurately reproducing the kinematic and straggling effects experienced by the scattered protons. The simulation's ability to calculate beam intensity solely from scattering data was later validated by comparing results from the simulation to the normal DRAGON procedure for a later ^{76}Se$(\alpha, \gamma)^{80}$Kr run [30, 31]. This experiment was chosen as it provided precise FC cup data and has an elastic cross section that could be accurately represented as purely Rutherford [32], therefore removing any systematic uncertainties in the input cross section data. Simulation results for the total integrated beam were subsequently observed to agree within 7% of those calculated using the canonical method.
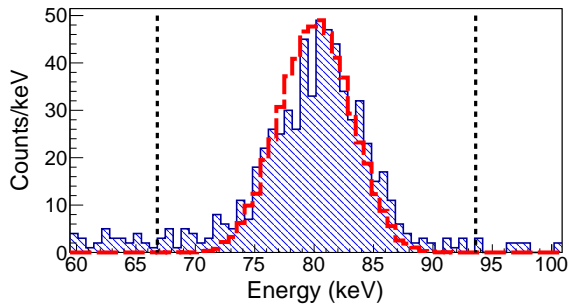

FIG. 5. Elastically scattered proton spectrum from the 30° silicon detector located in the target chamber. Experimental data are shown in striped solid (blue) with the simulation results overlayed as a dashed line (red). Simulation data were normalized to the height of the experimental data and the experimental data were calibrated in energy to the simulation data. Dashed vertical lines represent the cut placed on the experimental data when considering real elastically scattered proton events (color online).

E.   Particle identification

Three potential sources of background for the ^{19}Ne recoil runs were identified: ^{18}F beam particles that managed to pass through the recoil separator (referred to as *leaky beam*); ^{18}O leaky beam from beam contamination and ^{19}F recoil events from ^{18}O beam contamination. Attenuated beam runs allowed the locus of ^{18}F and ^{18}O events to be determined in a ΔE-ΔE plot from the IC, as displayed in Fig. 6. From this figure the ^{18}F attenuated beam events are visible in the larger locus, with the smaller locus being due to ^{18}O beam contamination.

There is a clear tailing effect below the ^{18}F peak, due to some of the incident ions scattering and losing energy in the detector gas volume. There are also high energy tails located to the right and above the main peak due to the piling up of sequential events. However, such pile up was not present during the recoil runs due to the low event rate.

During the runs where the separator was tuned to ^{19}Ne recoil nuclei, two events appeared in a region inconsistent with either ^{18}F or ^{18}O events (to the lower right of the ^{18}F locus in Fig. 6). As ^{19}Ne recoil events were expected to have a larger IC0 energy loss value than ^{18}F events, due to their larger atomic number and lower kinetic energy, these two events were hence considered ^{19}Ne recoil candidates. An additional three events appeared in the IC region corresponding to the ^{18}F locus. This number is not unexpected when the total beam intensity and DRAGON's typical suppression factor are considered; D'Auria *et al.* [24] reported a beam suppression factor of $\approx 10^{11}$ for DRAGON's EMS, in a similar mass and energy region, also with a (p,γ) reaction in inverse kinematics. However, due to the uncertainty in the region of the IC spectrum where ^{19}Ne recoil events were expected, these three events could also potentially have been recoils. This issue was resolved by observation of the MCP data which gave local TOF information on each particle via a time to amplitude converter (TAC) signal. Attenuated beam runs provided an expected TAC region where leaky beam particles would appear and the three suspected leaky ^{18}F events all had TAC values consistent with the ^{18}F region, to within 2σ. The two ^{19}Ne recoil candidates resided in a region with minimal background, calculated to be just 1.3×10^{-3} events per channel. This value was derived by considering ratios of events in attenuated beam and recoil runs for a given region, see Fig. 7 for the MCP TAC spectrum. The second peak in the attenuated beam data is most likely due to timing jitter or walk in the signal processing, affecting just 0.33% of the real peak events. Any recoils that experience this same effect would still be distinguishable from leaky beam however, in this spectrum and in Fig. 6.

Due to the fact that ^{19}F recoil ions from the ^{18}O$(p,\gamma)^{19}$F run had a speed indistinguishable from that of the ^{19}Ne recoil events from the ^{18}F$(p,\gamma)^{19}$Ne run (as the beam energies involved were identical and their kinematics were very similar) the MCP TAC data from the ^{18}O$(p,\gamma)^{19}$F run provided a region where ^{19}Ne recoil events were to be expected. Analysis of the relevant MCP TOF data revealed that ^{19}F recoil ions did appear in the same region as the two ^{19}Ne recoil candidates, as shown in Fig. 8. ^{19}F events were identified as they were coincident with a γ-ray decay event in the BGO array surrounding DRAGON's gas target. It can also be seen that the ^{18}O attenuated beam events appear in the same region as the ^{18}F attenuated beam events, indicating that the TAC scale remained consistent for both beam runs.

The IC spectrum from the ^{18}O run is shown in Fig. 9 together with the position of the two ^{19}Ne recoil events
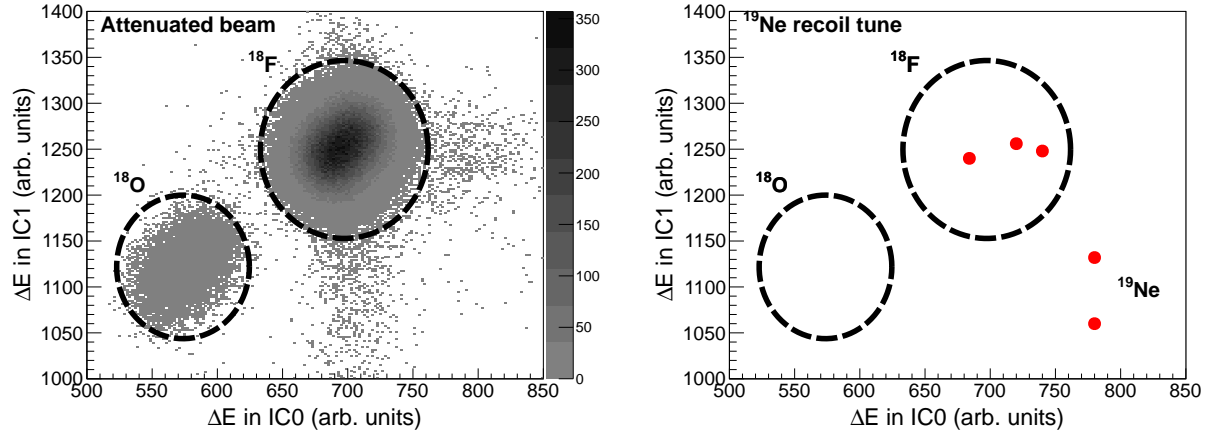
FIG. 6. Particle identification spectra from the IC anodes for a ^{18}F attenuated beam run (left) and the ^{19}Ne recoil runs (right, same axis). The attenuated beam runs exhibited two distinct loci coresponding to ^{18}F and ^{18}O ions (dashed circles). Of the five events observed in this region during the ^{19}Ne recoil runs (solid circles, red), three were located in an area consistent with the ^{18}F locus. Two events, however, resided in a region not consistent with either the ^{18}F or ^{18}O loci and were designated as ^{19}Ne recoil candidates, see text for details (color online).
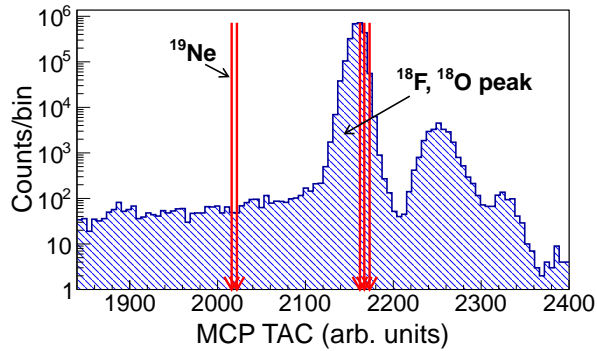
FIG. 7. MCP TAC spectrum showing where ^{18}F was observed during the attenuated beam run (striped, blue), together with the five observed events when tuned to ^{19}Ne recoils (arrows, red). The three ^{18}F events during the recoil run were clearly identified as they appeared in the same TAC region as the ^{18}F peak during the attenuated beam runs. The two ^{19}Ne recoil candidates appeared in a region of very low background however (color online).

FIG. 8. MCP TAC spectrum showing where ^{18}O was observed during the ^{18}O attenuated beam run (striped, blue), together with the observed ^{19}F recoil events (shaded, red). The scale is the same as that in Fig. 7. ^{19}F events were identified as they were accompanied by a coincident γ-ray event in the BGO array sourounding DRAGON's gas target. The ^{19}F recoil TAC region is consistent with that for the two ^{19}Ne recoil candidates, see text for details (color online).

from the ^{18}F beam data. Analysis of the silicon detector data together with the isobaric contamination ratio for these runs allowed the expected number of background events from ^{18}O$(p,\gamma)^{19}$F to be calculated. Only 0.40 background ^{19}F events were expected in total and a negligible fraction of them were expected to appear near the ^{19}Ne recoil events in the ^{18}F$(p,\gamma)^{19}$Ne data; of the 185 ^{19}F events seen in Fig. 9, none had a IC0 value high enough to be consistent with either of the ^{19}Ne events.

The level of isobaric contamination from ^{18}O was measured, at regular intervals, by sending attenuated beam directly into the I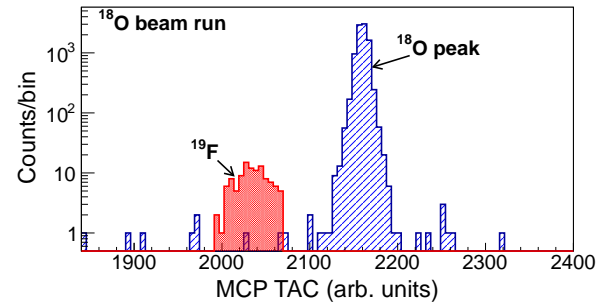C and measuring the ratio of peaks due to ^{18}O and ^{18}F (see Fig. 6). The ^{18}O:^{18}F ratio was observed to decrease from 1:20 to 1:260 throughout the experiment, as the residual gas in the ion source diminished. The positions of the ^{18}O and ^{18}F peaks in the IC spectrum were reproduced each time, and the position of the ^{18}O peak was in good agreement with the peak from the ^{18}O beam runs.

There were also events in the low energy region of the IC spectrum corresponding to particles scattered inside the recoil separator, changing charge state and losing momentum, that were able to reach the IC via a longer path involving several scattering events with device components. As they appeared far away from the leaky beam and recoil loci they did not contribute to the region of
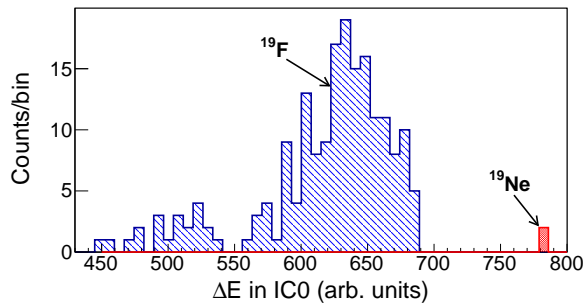
FIG. 9. Signal size spectra from the IC's first anode showing the position of $^{18}O(p,\gamma)^{19}F$ events from the ^{18}O beam run (striped, blue) together with ^{19}Ne events from the ^{18}F beam run (shaded, red). Less than one ^{19}F recoil event was expected to appear during the $^{18}F(p,\gamma)^{19}Ne$ run and so they were considered a negligible source of background in the ^{19}Ne recoil data, see text (color online).

TABLE I. BGO γ-ray detection efficiencies (ϵ_{BGO}) obtained from the Geant4 simulation for states in ^{19}F in the excitation region close that that populated during the $^{18}F(p,\gamma)^{19}Ne$ run. Level decay schemes taken from Ref. [34].

^{19}F level	ϵ_{BGO}
Ground state	62%
6927 keV	66%
7166 keV	87%

interest.

F. BGO array efficiency

Neither of the potential ^{19}Ne recoils had a coincident γ-ray detected in the BGO array which is often used as an additional means of background suppression. Lack of ^{19}Ne level decay scheme data for the excited state corresponding to the $E_{cm}=665$ keV resonance also made predicting the BGO efficiency difficult. A Geant4 simulation was used with γ-ray cascades assumed from ^{19}F states in an excitation region near to that populated in the ^{18}F run ($E_x=7066\rightarrow7090$ keV). The results are presented in table I and, once the BGO live time for the run (98.2%) is taken into account, give a minimum and maximum detection efficiency of 61% and 85%, respectively. In the absence of a statistical confidence interval, these results provide us with a range as to what BGO efficiency could be realistically expected from the experiment. As only two events in the recoil region were observed, the lack of γ-heavy ion coincidence events is consistent with the observed singles yield; assuming the minimum value of the array's calculated detection efficiency, there was a 15% chance of two consecutive recoil events not being detected by the array.

TABLE II. BGO γ-ray detection efficiencies (ϵ_{BGO}) obtained from the Geant4 simulation for states populated during the $^{18}O(p,\gamma)^{19}F$ run. Level decay schemes taken from Ref. [34].

^{19}F level	ϵ_{BGO}
Ground state	63%
8629 keV	74%
8650 keV	71%

In order to gain confidence in the BGO simulation's ability to determine γ-ray detection efficiencies in this mass and energy region, further analysis was conducted using the $^{18}O(p,\gamma)^{19}F$ run data. Placing a gate on the MCP time of flight data, together with IC ΔE data, allowed for recoil events to be discerned in both singles and coincidence data sets. A γ-ray detection efficiency was then determined by dividing the total number of coincidence recoil events by the total number of recoil events (The coincident event count also has to include the γ-ray array live time, in this case 95.4%). The γ-ray detection efficiency was subsequently calculated to be 69.9$\pm$3.8% for the ^{18}O run. This compares favorably with the simulation's results, which were done for a purely ground state transition and the two nearest states (8629 and 8650 keV) to the excitation energy range accessible within the target (8654$\rightarrow$8675 keV). The efficiency calculations are displayed in table II and the level decay schemes were taken from Ref. [34]. As the experimentally determined value lies within the range of the simulation results, confidence was gained in the simulation's ability to estimate γ-ray detection efficiencies for ^{19}Ne in this energy region. Hence, observing two ^{19}Ne recoil events with no coincident γ-ray event in the BGO array, as was the case in our experiment, was a perfectly plausible scenario.

G. Profile likelihood technique

All of the aforementioned techniques and data cuts gave a high confidence that the two events observed were both ^{19}Ne recoils, in a region of negligible background. A detected recoil count of $N_r^{det}=2.0^{+4.5}_{-1.7}(^{+1.8}_{-1.1})$ was calculated, at the 95% (68%) confidence level, using the profile likelihood technique outlined in Ref. [35]. This process involved characterizing the likelihood function for the data, including the parameters of interest as well as nuisance variables such as the various detection efficiencies given in Eqn. 2 (A list of the major nuisance parameters is given in table III). For this analysis the signal and background were treated as Poisson distributions whilst the beam normalization, detector efficiencies and other nuisance parameters were modeled as Gaussian. The relative magnitude of the systematic uncertainties in the various nuisance parameters are given in table III. The profile likelihood, given as λ, gave the like-

TABLE III. List of systematic experimental uncertainties.

Source of uncertainty	Uncertainty
Beam normalization	±12%
Target stopping power	±8.4%
End detection efficiency	±7.2%
Target length	±3.3%
Charge state distribution	±4.7%

lihood of observing the given parameter of interest as a function of that parameter only, whilst still accounting for the presence of nuisance parameters. This function was then used to extract limits on the parameter of interest, N_r^{det}. In this case a 95% (68%) confidence interval on N_r^{det} was extracted by taking the limits where the distribution increases by 3.84 (1.00) from the minimum. When the relevant function is plotted, as in Fig. 10, it can be clearly seen that the result was not statistically consistent with zero at either confidence level.
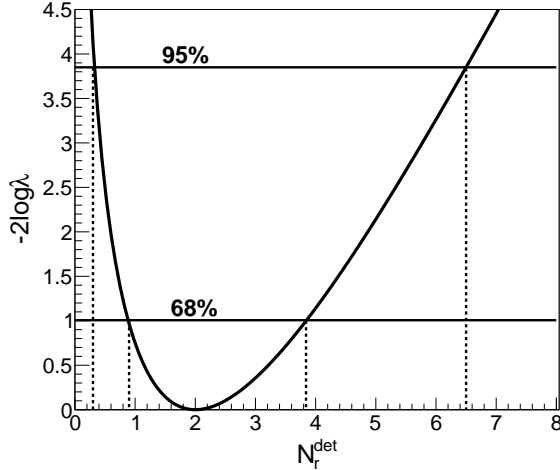

FIG. 10. Profile likelihood function for the number of ^{19}Ne recoil events detected, N_r^{det}. The dashed vertical lines show where the function increases by 3.84 (1.00), relative to the minimum, corresponding to a 95% (68%) confidence interval. A value of $2.0^{+4.5}_{-1.7}(^{+1.8}_{-1.1})$ for N_r^{det} was therefore adopted.

H. Strength of resonance at $E_{c.m.}$=665 keV

A resonance strength ($\omega\gamma$) of $26^{+59}_{-22}(^{+24}_{-14})$ meV and a Γ_γ of $101^{+226}_{-86}(^{+91}_{-55})$ meV were consequently calculated, at the 95% (68%) confidence level, both of which are a factor of ten smaller than the values assigned before this experiment. These values are improved from those reported previously from analysis of the same data [19], albeit by a margin small enough that it does not alter the original conclusions drawn. The main reason for this

improvement is the updated analysis of the MCP and IC detector efficiencies. The target energy loss was also re-evaluated with a more recent SRIM library. In addition, the implementation of Geant4 libraries and a reduction in the estimated magnitude of the elastic scattering cross section data in the elastic scattering simulation contributed to the revised resonance strength. Lastly, the BGO detector hardware threshold previously used in the Geant4 simulation was found to be lower than that observed in the data and so the array's efficiency for detecting prompt γ-ray events presented here differs from that reported previously.

I. Reaction rate analysis

An updated ^{19}Ne level scheme was used for the reaction rate analysis, taking into account the recent work by both Laird et al. [17] and Bardayan et al. [18]. The 665 keV resonance's contribution to the total reaction rate was calculated, with both the previous experimental upper limit and current results, in order to fully comprehend the impact of the current study. Cross sections were calculated within an R-matrix framework, including the external capture component and interference between resonances. The program AZURE2 [36] provided a convenient, user friendly interface with which to conduct this work. The calculation of reaction rates required numerical integration, as the narrow resonance formula did not account for the large width of the 665 keV resonance, nor the interference effects with lower lying states that affected the reaction cross section at lower energies. Hence the reaction rate was calculated according to:

$$N_A\langle\sigma v\rangle = 3.7318 \times 10^{10}\mu^{-1/2}T^{-3/2}\times$$
$$\int_0^\infty E_{c.m.}\sigma(E)e^{-11.605E_{c.m.}/T}\,dE \quad (7)$$

where $N_A\langle\sigma v\rangle$ is the product of the Avogadro constant and the reaction rate per particle pair in units of mol^{-1}s^{-1}cm^3 and μ is the reduced mass in atomic mass units. $E_{c.m.}$, T and σ are in units of MeV, GK and barn respectively [28].

This method required a large number of experimental parameters however, and there have been a number of studies characterizing the level scheme in the relevant region of ^{19}Ne, some of which have provided conflicting results. Here, level parameters were taken primarily from those published in the recent work by Bardayan et al. [18], whose data is a weighted average of both their own work and that done by Laird et al. [17], with certain level parameters adapted from Adekola et al. [10] (see Ref. [18] for the complete discussion). A few additional states were also taken from data in the review by Nesaraja et al. [14]. See table IV for the complete resonance parameter list. A direct capture component was also included, approximated to be 2.4×10^{-3} MeV b

from Ref. [7]. The scenario that maximized the 665 keV resonance's potential contribution to the total reaction rate was first considered when selecting the phase interference between states, in order to fully appreciate the potential significance of the current study. The scenario corresponding to minimizing the 665 keV resonances contribution was also investigated such that the full range of possible outcomes from this work could be appreciated.

The calculated S-factors for ^{18}F(p,γ) are displayed in Fig. 11. Using the strength for the resonance at 665 keV measured in this work, compared to the previous upper limit from Rehm *et al.* [13], a significant drop in the calculated S-factor at a range of energies is clearly observed. Graph (a) in Fig. 12 displays the 665 keV resonant contribution to the total reaction rate at nova temperature, using the previous experimental upper limit. Although the 330 keV resonance (E_x=6.741 MeV) does dominate, only the Γ_p of the E_x=6.741 MeV state has been experimentally determined [16] and the model calculations are based on Γ_γ and Γ_α from an assumed analogue assignment [7]. Another state with the same J$^\pi$, but different width, does lie nearby so this assignment is by no means definitive, meaning that the 665 keV resonance could have played a major role in this temperature range (0.1→0.4 GK). It can be clearly seen in both Graph (b) and (c) of Fig 12 that, compared to the 330 keV resonance, only now can it be definitively shown that this resonance makes no significant contribution to the reaction rate at any temperature relevant to novae. Tabulated reaction rate values are provided in Table V.

IV. SUMMARY

The strength of the 665 keV resonance in the ^{18}F(p,γ)^{19}Ne reaction has been measured, in inverse kinematics, using the recoil mass separator DRAGON. Two ^{19}Ne recoil events were discerned with a high confidence and the resulting $\omega\gamma$ is a factor of ten smaller than the previous assignment of 1 eV [14] and a factor of thirty smaller than the previous experimental upper limit [13]. Hence, although our Γ_γ measurement is consistent with the previous experimental upper limit, it is still significantly lower than previously thought. As a consequence this resonance has been shown experimentally to play a significantly diminished role in the destruction of ^{18}F at temperatures associated with ONe novae, and thus only has a trivial influence on the ^{18}F abundance after the resulting outburst. It is therefore now clear that either a direct measurement of the 330 keV resonance or an indirect determination of the Γ_γ and Γ_α of the associated state, together with more accurate knowledge of the ^{19}Ne level scheme, is crucial if future ^{18}F abundance observations are to be fully exploited. Note that although the $\omega\gamma$ and Γ_γ given here differ from those reported previously from the same data [19], the original conclusions drawn from that work remain unchanged.

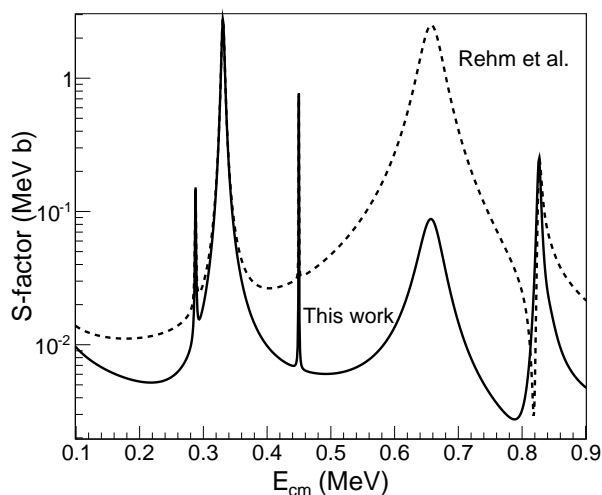FIG. 11. Comparison of the calculated ^{18}F(p,γ)^{19}Ne S-factors using both the Rehm *et al.* upper limit (dashed) and this work (solid) for the 665 keV resonance's strength. Although the Gamow window in novae is below 300 keV, the resonance at 665 keV is so broad that its low energy tail still has an influence in this region. The level parameter's phase interference was configured to maximize the 665 keV resonance's influence; see text.

TABLE IV. ^{19}Ne level scheme adopted for the R-Matrix calculation. Γ_γ widths set to 1 eV are assumed based purely on nearby analogue states in ^{19}F.

E_x (MeV)	E_r (keV)	J^π	Γ_γ (eV)	Γ_p (keV)	Γ_α (keV)	Ref.
6.286	-124	$^1\!/_2{}^+$	1	83.5[a]	11.6	[18]
6.417	7	$^3\!/_2{}^-$	1	1.6×10^{-41}	0.5	[18]
6.439	29	$^1\!/_2{}^-$	1	3.8×10^{-19}	220	[18]
6.457	47	$^3\!/_2{}^+$	1	2.1×10^{-13}	1.3	[18]
6.699	289	$^5\!/_2{}^+$	0.29	2.4×10^{-5}	1.2	[18]
6.742	332[b]	$^3\!/_2{}^-$	5.0[c]	2.2×10^{-3}	5.2	[18]
6.861	450	$^7\!/_2{}^-$	2.3	1.1×10^{-5}	1.2	[14]
7.075	664.7	$^3\!/_2{}^+$	3[d]&0.101[e]	15.2	23.8	[18]
7.238	827	$^3\!/_2{}^+$	1	0.35	6.0	[14]
7.253	842	$^1\!/_2{}^+$	1	0.2	23	[14]

[a] ANC in fm$^{-1/2}$
[b] Referred to as the 330 keV resonance in the text
[c] Negative (positive) phase chosen to maximize (minimize) influence of 665 keV resonance, see text
[d] Experimental upper limit taken from Rehm *et al.* [13], two widths used for comparison, see text for details
[e] This work, positive (negative) phase chosen to maximize (minimize) influence of 665 keV resonance, see text

TABLE V. ^{18}F$(p,\gamma)^{19}$Ne reaction rate data calculated using the present work, with the 665 keV resonance's contribution maximized. Upper and lower rates corespond to a variation in the $E_{c.m.}$=665 keV resonance's Γ_γ at the 95% confidence interval.

| T (GK)	Lower (cm^{3}mol^{-1}sec^{-1})	Median (cm^{3}mol^{-1}sec^{-1})	Upper (cm^{3}mol^{-1}sec^{-1})
0.03	2.42×10^{-16}	2.42×10^{-16}	2.42×10^{-16}
0.04	2.45×10^{-14}	2.45×10^{-14}	2.46×10^{-14}
0.05	4.82×10^{-13}	4.84×10^{-13}	4.88×10^{-13}
0.06	4.67×10^{-12}	4.70×10^{-12}	4.78×10^{-12}
0.07	3.13×10^{-11}	3.16×10^{-11}	3.24×10^{-11}
0.08	1.63×10^{-10}	1.65×10^{-10}	1.70×10^{-10}
0.09	6.86×10^{-10}	6.97×10^{-10}	7.23×10^{-10}
0.1	2.43×10^{-9}	2.47×10^{-9}	2.58×10^{-9}
0.11	7.42×10^{-9}	7.58×10^{-9}	7.94×10^{-9}
0.12	2.02×10^{-8}	2.06×10^{-8}	2.17×10^{-8}
0.13	4.97×10^{-8}	5.09×10^{-8}	5.38×10^{-8}
0.14	1.14×10^{-7}	1.17×10^{-7}	1.24×10^{-7}
0.15	2.47×10^{-7}	2.54×10^{-7}	2.69×10^{-7}
0.16	5.22×10^{-7}	5.36×10^{-7}	5.69×10^{-7}
0.18	2.29×10^{-6}	2.35×10^{-6}	2.47×10^{-6}
0.2	9.91×10^{-6}	1.01×10^{-5}	1.05×10^{-5}
0.25	2.33×10^{-4}	2.35×10^{-4}	2.39×10^{-4}
0.3	2.27×10^{-3}	2.28×10^{-3}	2.31×10^{-3}
0.35	1.18×10^{-2}	1.18×10^{-2}	1.19×10^{-2}
0.4	4.03×10^{-2}	4.05×10^{-2}	4.10×10^{-2}
0.45	1.04×10^{-1}	1.05×10^{-1}	1.07×10^{-1}
0.5	2.22×10^{-1}	2.25×10^{-1}	2.32×10^{-1}
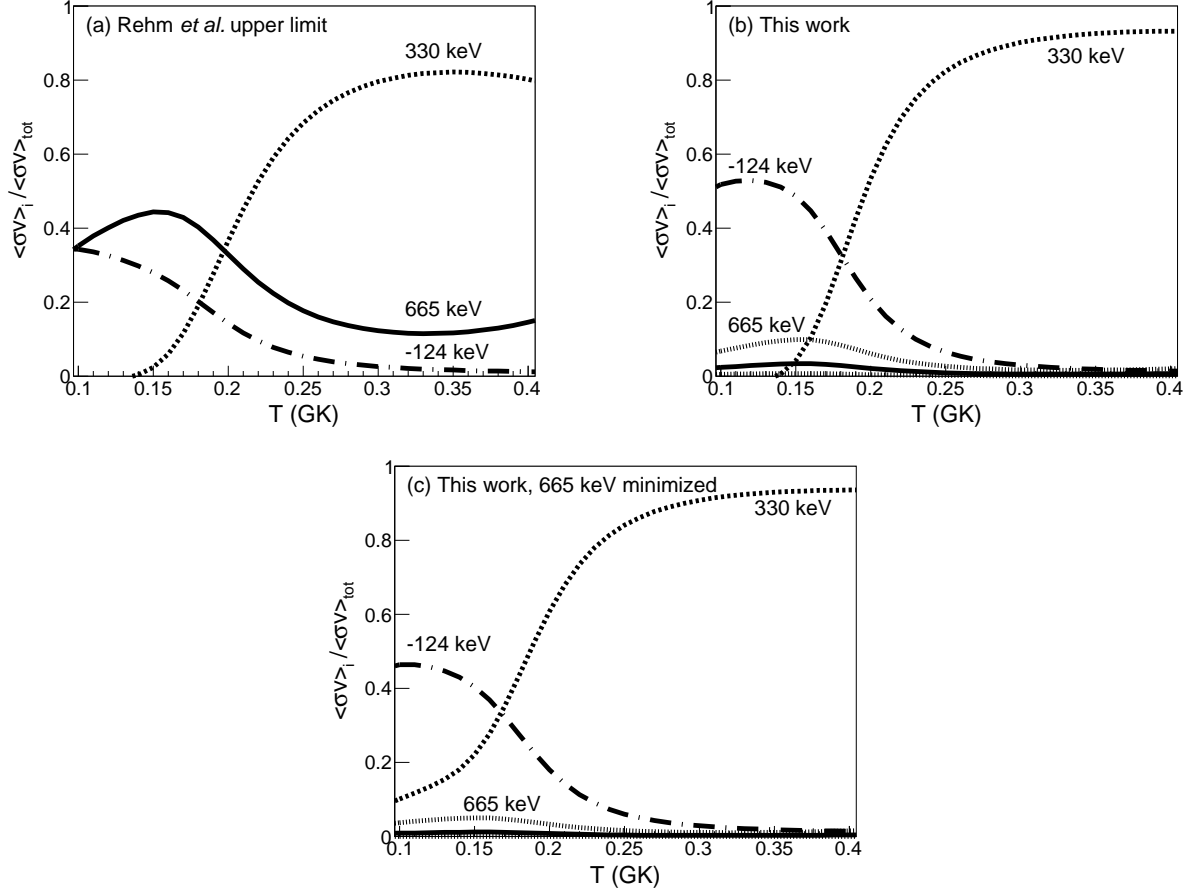
FIG. 12. Fractional resonant contributions to the total $^{18}\text{F}(p,\gamma)^{19}\text{Ne}$ reaction rate at as a function of temperature, in the peak nova range. Graph (a) shows the 665 keV rate (solid) using the experimental upper limit taken from Rehm *et al.* [13] whilst graph (b) has the rate using the current work. (a) and (b) both maximize the 665 keV resonances contribution through phase interference. Graph (c) displays the senario of minimizing the 665 keV resonance's contribution to the total rate through phase interference. Fine dashed lines represents the resulting uncertainty when varying our measured Γ_γ at the 95% confidence interval. The 330 keV resonance (dashed) and the sub-threshold -124 keV state (dash-dot) contributions were computed using data from Ref. [18]. Note that at lower temperatures lower lying resonances, together with the direct capture component account for the remaining contribution to the total rate.

[1] J. José and M. Hernanz, The European Physical Journal A - Hadrons and Nuclei **27**, 107 (2006).

[2] S. A. Grebnev, A. A. Lutovinov, S. S. Tsygankov, and C. Winkler, Nature **490**, 373 (2012).

[3] J. José and M. Hernanz, J. Phys. G **34**, R431 (2007).

[4] R. Diehl *et al.*, Nature **439**, 45 (2006).

[5] M. Hernanz, *Classical Novae (edited by M. F. Bode and A. Evans)*, 2nd ed. (Cambridge University Press, Cambridge, England, 2008).

[6] C. Iliadis, A. Champagne, J. José, S. Starrfield, and P. Tupper, The Astrophys. J. Suppl. Ser. **142**, 105 (2002).

[7] S. Utku, J. G. Ross, N. P. T. Bateman, D. W. Bardayan, A. A. Chen, J. Görres, A. J. Howard, C. Iliadis, P. D. Parker, M. S. Smith, R. B. Vogelaar, M. Wiescher, and K. Yildiz, Phys. Rev. C **57**, 2731 (1998).

[8] D. J. Mountford, A. S. J. Murphy, N. L. Achouri, C. Angulo, J. R. Brown, T. Davinson, F. de Oliveira Santos, N. de Séréville, P. Descouvemont, O. Kamalou, A. M. Laird, S. T. Pittman, P. Ujic, and P. J. Woods, Phys. Rev. C **85**, 022801 (2012).

[9] C. E. Beer, A. M. Laird, A. S. J. Murphy, M. A. Bentley, L. Buchmann, B. Davids, T. Davinson, C. A. Diget, S. P. Fox, B. R. Fulton, U. Hager, D. Howell, L. Martin, C. Ruiz, G. Ruprecht, P. Salter, C. Vockenhuber, and P. Walden, Phys. Rev. C **83**, 042801 (2011).

[10] A. S. Adekola *et al.*, Phys. Rev. C **83**, 052801 (2011).

[11] A. Coc, M. Hernanz, J. Jose, and J.-P. Thibaud, Astron.Astrophys. (2000), arXiv:astro-ph/0003166 [astro-ph].

[12] N. Shu, D. W. Bardayan, J. C. Blackmon, C. Yong-Shou, R. L. Kozub, P. D. Parker, and M. S. Smith, Chinese Physics Letters **20**, 1470 (2003).

[13] K. E. Rehm, C. L. Jiang, M. Paul, D. Blumenthal, L. A. Daniel, C. N. Davids, P. Decrock, S. M. Fischer, D. Henderson, C. Lister, J. Nickles, J. Nolen, R. C. Pardo, J. P. Schiffer, D. Seweryniak, and R. E. Segel, Phys. Rev. C **55**, R566 (1997).

[14] C. D. Nesaraja, N. Shu, D. W. Bardayan, J. C. Blackmon, Y. S. Chen, R. L. Kozub, and M. S. Smith, Phys. Rev. C **75**, 055809 (2007).

[15] D. W. Bardayan, R. L. Kozub, and M. S. Smith, Phys. Rev. C **71**, 018801 (2005).

[16] D. W. Bardayan, J. C. Batchelder, J. C. Blackmon, A. E. Champagne, T. Davinson, R. Fitzgerald, W. R. Hix, C. Iliadis, R. L. Kozub, Z. Ma, S. Parete-Koon, P. D. Parker, N. Shu, M. S. Smith, and P. J. Woods, Phys. Rev. Lett. **89**, 262501 (2002).

[17] A. M. Laird, A. Parikh, A. S. J. Murphy, K. Wimmer, A. A. Chen, C. M. Deibel, T. Faestermann, S. P. Fox, B. R. Fulton, R. Hertenberger, D. Irvine, J. José, R. Longland, D. J. Mountford, B. Sambrook, D. Seiler, and H.-F. Wirth, Phys. Rev. Lett. **110**, 032502 (2013).

[18] D. Bardayan, K. Chipps, S. Ahn, J. Blackmon, R. de-Boer, U. Greife, K. Jones, A. Kontos, R. Kozub, L. Linhardt, B. Manning, M. Matoš, P. O'Malley, S. Ota, S. Pain, W. Peters, S. Pittman, A. Sachs, K. Schmitt, M. Smith, and P. Thompson, Phys. Lett. B **751**, 311 (2015).

[19] C. Akers, A. M. Laird, B. R. Fulton, C. Ruiz, D. W. Bardayan, L. Buchmann, G. Christian, B. Davids, L. Erikson, J. Fallis, U. Hager, D. Hutcheon, L. Martin, A. S. J. Murphy, K. Nelson, A. Spyrou, C. Stanford, D. Ottewell, and A. Rojas, Phys. Rev. Lett. **110**, 262502 (2013).

[20] D. A. Hutcheon *et al.*, Nucl. Instrum. Methods A **498**, 190 (2003).

[21] C. Vockenhuber, C. O. Ouellet, L.-S. The, L. Buchmann, J. Caggiano, A. A. Chen, H. Crawford, J. M. D'Auria, B. Davids, L. Fogarty, D. Frekers, A. Hussein, D. A. Hutcheon, W. Kutschera, A. M. Laird, R. Lewis, E. O'Connor, D. Ottewell, M. Paul, M. M. Pavan, J. Pearson, C. Ruiz, G. Ruprecht, M. Trinczek, B. Wales, and A. Wallner, Phys. Rev. C **76**, 035801 (2007).

[22] C. Vockenhuber, L. Erikson, L. Buchmann, U. Greife, U. Hager, D. Hutcheon, M. Lamey, P. Machule, D. Ottewell, C. Ruiz, and G. Ruprecht, Nucl. Instrum. and Meth. A **603**, 372 (2009).

[23] C. Vockenhuber, L. Buchmann, J. Caggiano, A. Chen, J. DAuria, C. Davis, U. Greife, A. Hussein, D. Hutcheon, D. Ottewell, C. Ouellet, A. Parikh, J. Pearson, C. Ruiz, G. Ruprecht, M. Trinczek, and J. Zylberberg, Nucl. Instrum. and Meth. B **266**, 4167 (2008).

[24] J. M. D'Auria, R. E. Azuma, S. Bishop, L. Buchmann, M. L. Chatterjee, A. A. Chen, S. Engel, D. Gigliotti, U. Greife, D. Hunter, A. Hussein, D. Hutcheon, C. C. Jewett, J. José, J. D. King, A. M. Laird, M. Lamey, R. Lewis, W. Liu, A. Olin, D. Ottewell, P. Parker, J. Rogers, C. Ruiz, M. Trinczek, and C. Wrede, Phys. Rev. C **69**, 065803 (2004).

[25] P. G. Bricault, F. Ames, M. Dombsky, F. Labrecque, J. Lassen, A. Mjos, G. Minor, and A. Tigelhoefer, Rev. Sci. Instrum. **83**, 02A914 (2012).

[26] P. W. Schmor, *AIP Conference Proceedings **473**, 439 1999.*

[27] W. Liu, G. Imbriani, L. Buchmann, A. Chen, J. D'Auria, A. D'Onofrio, S. Engel, L. Gialanella, U. Greife, D. Hunter, A. Hussein, D. Hutcheon, A. Olin, D. Ottewell, D. Rogalla, J. Rogers, M. Romano, G. Roy, and F. Terrasi, Nucl. Instrum. Methods A **496**, 198 (2003).

[28] C. Iliadis, *Nuclear Physics of Stars* (John Wiley and Sons, Weinheim, Germany, 2007).

[29] J. F. Ziegler, M. Ziegler, and J. Biersack, Nucl. Instrum. Methods B **268**, 1818 (2010).

[30] C. Akers, Ph.D. thesis, University of York (2014).

[31] J. Fallis *et al.*, in *XIII Nuclei in the Cosmos, Proceedings of Science* 2014.

[32] T. Rauscher, N. Dauphas, I. Dillmann, C. Fröhlich, Z. Fülöp, and G. Gyürky, Rep. Prog. Phys. **76**, 066201 (2013).

[33] G. F. Knoll, *Radiation Detection and Measurement*, 3rd ed. (John Wiley & Sons, 2000).

[34] D. Tilley, H. Weller, C. Cheves, and R. Chasteler, Nucl. Phys. A **595**, 1 (1995).

[35] W. A. Rolke, A. M. López, and J. Conrad, Nucl. Instrum. Methods A **551**, 493 (2005).

[36] R. E. Azuma, E. Uberseder, E. C. Simpson, C. R. Brune, H. Costantini, R. J. de Boer, J. Görres, M. Heil, P. J. LeBlanc, C. Ugalde, and M. Wiescher, Phys. Rev. C **81**, 045805 (2010).